Food and Chemical Toxicology 144 (2020) 111633

Contents lists available at ScienceDirect

Food and Chemical Toxicology

journal homepage: www.elsevier.com/locate/foodchemtox

A rapid and convenient screening method for detection of restricted monensin, decoquinate, and lasalocid in animal feed by applying SERS and chemometrics

Kyung-Min Lee [a,*], Danielle Yarbrough [b], Mena M. Kozman [c], Timothy J. Herrman [a], Jinhyuk Park [d], Rui Wang [e], Dmitry Kurouski [e]

[a] Office of the Texas State Chemist, Texas A&M AgriLife Research, Texas A&M University System, College Station, TX, 77843, United States
[b] Department of Chemical Engineering, Texas A&M University, College Station, TX, 77843, United States
[c] Department of Biology, Texas A&M University, College Station, TX, 77843, United States
[d] Department of Biological and Agricultural Engineering, Texas A&M University, College Station, TX, 77843, United States
[e] Department of Biochemistry and Biophysics, Texas A&M University, College Station, TX, 77843, United States

ARTICLE INFO

Keywords:
Surface-enhanced Raman spectroscopy (SERS)
Chemometrics
Antimicrobials
Gold nanoparticles
Food safety

ABSTRACT

The surface-enhanced activities of size- and shape-controlled gold nanoparticles (AuNPs) with superior chemical stability were investigated to explore a possible development of a simple and non-destructive spectroscopic method to help the regulatory agency's analytical services for rapid detection and characterization of selected antimicrobials in animal feeds. Feed samples spiked at different concentration ranges of antimicrobials were evaluated using AuNPs as a surface-enhanced Raman spectroscopy (SERS) agent. The collected SERS spectra were mathematically preprocessed for further analysis. The classification models obtained 100% predictive accuracy with zero or little misclassification. The first two canonical variables ($p = 0.001$) could explain >95% of the variability in preprocessed spectral data. Most chemometric models for predicting MON, DEC, and LAS concentrations showed a high predictive accuracy ($r^2 > 0.90$), lower predictive error (<20 mg/kg), and satisfactory regression quality (slope close to 1.0). The statistical results showed no statistically significant difference between the reference and SERS predicted values ($p > 0.05$). The findings and implications from the study indicate that SERS would be a powerful and efficient technique possessing a great potential serving as an excellent monitoring and screening tool for antimicrobial contaminated samples in the on-site analysis.

1. Introduction

Raman spectroscopy is a vibrational spectroscopic technique for the rapid identification of chemical and biological molecules based on the scattering effect of the molecules (Smith and Dent, 2005). Raman spectroscopy is more sensitive to the polarizability of symmetrical covalent bonds in non-polar functional groups, producing well-resolved bands of a target molecule and its derivatives. However, its major shortcoming is a small cross-section and low efficiency of Raman scattering, resulting in a lack of sensitivity for the target analyte. Surface-enhanced Raman spectroscopy (SERS) is an advanced Raman technique which improves the weak Raman scattering efficiency of molecules adsorbed on or at the vicinity of rough metal surfaces through a surface plasmon resonance effect of metal nanoparticles (Craig et al., 2013). The suitability and efficiency of SERS are largely determined by its preparation methods, including chemical reduction, electro/physical deposition of nanoparticles, and thermal decomposition (Fan et al., 2011). SERS enhancement factors reported in previous works are typically in the range of 10^4 to 10^{10} and even up to extremely high enhancement levels enough for detection and orientation of a single molecule (Craig et al., 2013). The SERS enhancement and intensity is believed to be dependent on a local substrate morphology, which is considered to influence the effect of surface resonance (Lee and Herrman, 2016; Plieth et al., 2005). The theories to explain the Raman enhancement effect generating from randomly distributed "hot spots" (a gap between nanoparticles) are based on the two suggested mechanisms: electromagnetic (EM) mechanism and charge transfer mechanism (Craig et al., 2013; Haynes et al., 2005). According to the EM mechanism, upon

* Corresponding author.
E-mail address: kml@otsc.tamu.edu (K.-M. Lee).

https://doi.org/10.1016/j.fct.2020.111633
Received 4 June 2020; Received in revised form 3 July 2020; Accepted 17 July 2020
Available online 30 July 2020
0278-6915/Published by Elsevier Ltd.

illumination by the light of a particular excitation wavelength, the incoming photon interacts with the metallic nanoparticles within which the conduction electrons oscillate, leading to the surface plasmon resonance of dipole oscillation. This produces large-local electromagnetic fields, resulting in an enhanced Raman emission. The Raman enhancement is further amplified by the surface plasmon excitation of the substrate. The charge transfer mechanism involves the formation of an electric field due to electron transfer between the adsorbed molecule and the metal nanoparticle which can shift the frequency of the scattered photon and have an additional Raman enhancement effect (Plieth et al., 2005).

For the last decades, there have been great efforts for the systematic development of well-engineered SERS substrates and the improved understanding of the conditions to produce enhanced SERS signals. However, the SERS technique as a reliable and accurate analytical tool still seems to have some issues and obstacles to overcome. The extensive application for a simple field deployment as a reliable screening method is still limited because most current SERS techniques rely on laborious extraction procedures, complex manufacturing processes, and complex chemometric techniques (Haynes et al., 2005). Besides, the results from SERS measurements are often irreproducible because of the morphological variation of nanostructures and target-adsorption variability (Lee and Herrman, 2016; Yuan et al., 2009). Chemometric methods have been applied to facilitate spectral data processes and correlate actual chemical and process measurements to the spectral data through diverse statistical and mathematical procedures and tools (Cramer, 1993; Delwiche and Hareland, 2004). So such techniques allow us to better understand and interpret the spectral data by greatly simplifying the complex data structure to find a piece of hidden information and test a hypothesis (Johnson, 1998; Osborne et al., 1993). The chemometric methods can be categorized into 1) the design of experiments such as factor screening, 2) data preprocessing such as normalization, baseline correction, and derivatization, 3) qualitative analysis/classification such as unsupervised or supervised pattern recognition methods, and 4) calibration such as artificial neural network and partial least squares (Lee et al., 2005; Moros et al., 2010; Roggo et al., 2007).

Plasmon-enhanced phenomena in gold nanoparticles (AuNPs) for SERS detection of a variety of analytes have been an interesting and challenging research subject for the last decades (Amendola et al., 2017; Athukorale et al., 2019). Table 1 summarizes the application of gold and silver nanoparticles as SERS agents used in the previous studies. The Raman scattering efficiency can be greatly improved if target molecules are deposited close to plasmonic AuNP substrates (Jahn et al., 2016). Despite the controversial hypotheses, the charge-transfer metal--molecule is considered as one of the main effects that are responsible for resonantly-enhanced Raman signal (Lombardi and Birke, 2009). A high enhancement effect of Raman scattering can be obtained from a single hot-spot between two Au spheres and largely depends on the gap size (Moskovits, 2005; Simoncelli et al., 2016). In the local-field enhancement of Raman scattering, the AuNP substrate increases the light intensity at the metal surface as well as enhances Raman scattering effect from target molecules (Di Fabrizio et al., 2016). It's generally accepted that the Raman enhancement effect in AuNP substrate is maximized when the wavelength of excitation and Raman scattering photons is within the profile of surface plasmon resonance of gold nanoparticles (Amendola et al., 2017). The local electromagnetic field decays substantially with distance from the surface of AuNP so the Raman enhancement effect may dramatically reduce from the surface (Joshi et al., 2016). This indicates that molecules located in the first layers adjacent to the metal surface could determine the Raman enhancement effect (Compagnini et al., 1999). Multiple factors can influence plasmon-enhanced phenomena, of which the size, structure, and morphology of AuNPs have been intensively studied for their effects on physicochemical properties because they can substantially affect the degree of enhancement of local electromagnetic fields and its use as SERS agents (Bastús et al., 2011; Bigall et al., 2008). The surface-enhancement activities of AuNPs are in general lower than those of silver nanoparticles (Athukorale et al., 2019). But the AuNPs for SERS is often preferred because it can provide better chemical stability and higher biocompatibility (Amendola et al., 2017; Bastús et al., 2011).

Table 1
Gold (Au) or silver (Ag) nanoparticles-based SERS sensors applied for detection of selected target analytes in various matrices.

Sensor type	Sample matrix	Target analyte	Limit of detection	References
Molecularly imprinted polymer-AuNPs	Rice and wheat	Prometryn and simetryn	20 μg/kg	Yan et al. (2019)
Spheroidal AuNPs	Pome fruits	Pyrimethanil	4.74 mg/kg	Mandrile et al. (2018)
Spheroidal AuNPs	Fish muscle	Trace methylene blue	10 ng/g	Li et al. (2016)
Spheroidal AuNPs	Tea	Carbendazim	100 μg/kg.	Chen et al. (2019)
Spheroidal AuNPs	Apple	Chlorpyrifos	0.13 mg/kg	Chen et al. (2015)
Ultrafiltration membrane-AuNPs	Orange extract	Thiabendazole	0.125 μg/g	Hong et al. (2017)
Spheroidal AuNPs	Apple juice	Paraquat	0.2 μg/L	Luo et al. (2018)
Flower-shaped AgNPs	Water	Carmine	10^{-8} M.	Wu et al. (2017)
Spheroidal AgNPs	Pear	Alternariol	1.30 μg/L	Pan et al. (2018)
Molecularly imprinted polymers-colorimetric AgNPs	Apple juice	Chlorpyrifos	0.01 mg/L	Feng et al. (2017)
Chitosan-modified AgNPs	Milk powder	Melamine; dicyandiamide; sodium sulfocyanate	1 mg/L; 100 mg/L; 10 mg/L	Li et al. (2017)

Monensin (MON), lasalocid (LAS), and decoquinate (DEC) have been used as coccidiostats in poultry and as growth promoters in swine and cattle (Clarke et al., 2014). Of these coccidiostats, MON and LAS belong to the ionophores group with complex and high molecular weight, derived from several Streptomyces species (Harris et al., 1998). These ionophore antimicrobials readily form complexes with metal cations through hydrogen bonds (Chattopadhyay et al., 1992; Picquart, 2000). Such complexes can interact with phospholipids and cross cell membranes with the help of the gradients in cation concentration and pH. MON carries Na + ions more efficiently while LAS seems more appropriate for transporting K+ ions. Transporting metal cations across the cell membrane is the main action mode of MON and LAS, which can significantly affect the osmotic balance in the cell, causing the death of the parasite cell (Matabudul et al., 2002). DEC is a chemical coccidiostat and acts on a parasite cell differently from MON and LAS. DEC prevents the production of mitochondrial energy during the early stage of cell development (Clarke et al., 2014). There has been an increasing public concern on the misuse of these antimicrobials, particularly, the polyether ionophores which are believed to induce some damages on peripheral nerves and cardiac and skeletal muscles of animals (Oehme and Pickrell, 1999).[19] Such toxic consequences can occur when the antimicrobials are taken above the recommended levels or present in animal feeds not intended for particular species. For example, a therapeutic level of MON for chicken (121–150 mg/kg) in feed can cause intoxication for cattle and 20–50% of its overdosage may also show the first evidence of toxicity (Dowling, 1992; Matsuoka et al., 1996). Office of the Texas State Chemist (OTSC) is a regulatory body that oversights for about 5,000 feed firms distributing 23 million tons of feed products in Texas, US, and abroad. The agency also serves a large animal population including 900,000 dairy cows and 12.6 million cows and calves. As a

regulatory body, the agency needs to analyze large amounts of feed samples on a daily base including antimicrobial residues in animal feed, particularly MON, DEC, and LAS. Thus, the spectroscopic method including the SERS technique would provide a new innovative way of analyzing and effectively managing antimicrobials reissues in feed products to promote the feed safety and quality and protect the health of animals and humans.

A critical need exists to develop and implement accurate and reliable analytical methods for early detection and identification of the antimicrobials in different types of contaminated feed matrices at inclusion and trace levels for their quality control and regulation. Besides, it has been challenging to design the appropriate procedures of extraction, clean-up, and pretreatment of the sample matrices, particularly for multi-residue antimicrobial analysis before instrument evaluation (Bacanli and Başaran, 2019; Boscher et al., 2010). The current analytical methods widely used for the detection of antimicrobial residues in animal feed may be categorized into 1) relatively simple and inexpensive screening methods including microbiological assays and immunoassays (Kurittu et al., 2000; Weber et al., 2005) and 2) highly selective and sensitive confirmatory methods including liquid chromatography (LC) coupled to mass spectrometry (MS) (Mortier et al., 2005), capillary electrophoresis (CE) (García-Campaña et al., 2009), and LC with ultraviolet (UV) detection (Benito-Peña et al., 2009). Recently there have been also increasing interests in the application and benefit of automatic biosensors due to their high specificity and affinity to antimicrobial molecules (Bacanli and Başaran, 2019). However, it's worthwhile to note that the confirmatory methods are expensive and time-consuming and require large amounts of reagents, highly experienced personnel, and well-equipped laboratories. Meanwhile, the screening methods generally lack specificity and accuracy and offer only semi-quantitative results of antimicrobial residue. Simple and non-destructive spectroscopic methods such as infrared spectroscopy coupled with chemometric methods have demonstrated their ability to characterize and differentiate coccidiostats-containing feed additives with different formulations (Omar et al., 2015). For official antimicrobial analysis of animal feeds, the laboratories are necessary or recommended to be accredited and comply with the requirements according to ISO/IEC 17025:2017 to fulfill the quality parameters of the analytical methods (Separovic et al., 2019).

SERS technique is attractive and promising for rapid identification and characterization of restricted antimicrobials because it's simpler, faster, and more efficient than standard wet-chemical methods (He et al., 2010; Lai et al., 2011; Zhang et al., 2012a). This technique requires a small sample size, time-and cost-effective sample preparation for field operation, and simplified sample extraction protocols (Lai et al., 2011). Besides, the SERS method can provide useful and valuable information on molecular structure, reactivity, and conformation of antimicrobials (Olavarría-Fullerton et al., 2011). The presence and shift of characteristic peaks corresponding to vibrational modes of antimicrobial molecules are often used for identification of functional chemical groups and assessment of their binding properties with the metal surface as well as the determination of degradation products and derivatives of the antimicrobials (He et al., 2010; Lai et al., 2011; Olavarría-Fullerton et al., 2011). However, to our knowledge, there has been only a little research to analyze selected MON, DEC, and LAS antimicrobials in very complex animal feed matrices using vibrational spectroscopic methods. No one or little work has been done to evaluate the feasibility and possibility of a more sensitive SERS technique for qualitative and quantitative analysis of the antimicrobials in feed. Therefore, the purpose of the present study was to explore the feasibility of SERS technique based on a different type of gold nanoparticles in combination with chemometric algorithms to develop simple, rapid, and low-cost method for early detection and identification of three commonly used antimicrobials in animal feeds using an extract after performing a simple extraction step in the in-house methods developed for confirmatory HPLC analyses. The developed method was aimed to be able to screen antimicrobial contaminated feed samples at a level of concern of the regulatory agencies and consumers.

2. Materials and methods

2.1. Materials

Monensin (MON), decoquinate (DEC), and lasalocid sodium (LAS) were purchased from Sigma-Aldrich Co. (St. Louis, MO). All organic solvents, reagents, and chemicals employed in the extractions and for HPLC analysis were of analytical grade and used as received without any further purification.

2.2. Sample preparation

Non-contaminated beef cattle feeds with antimicrobials were obtained from the Office of the Texas State Chemist (OTSC) regulatory samples collected according to the state's sampling plan. The feed samples were spiked at different concentration ranges of MON (1.0, 5.0, 7.5, 10.0, 12.5, 15.0, 17.5, 20.0, 25.0, and 50.0 mg/kg), DEC (1.5, 3.0, 5.0, 10.0, 15.0, 20.0, 25.0, 50.0, 75.0, and 100.0 mg/kg), and LAS (2.5, 5.0, 10.0, 20.0, 30.0, 40.0, 50.0, 75.0, 100.0, and 150.0 mg/kg). The samples were then stored in a polyethylene bottle in a 4 °C refrigerator. Before biochemical and SERS spectroscopic analyses, the samples were equilibrated at room temperature for at least 1 h.

2.3. Sample extraction and HPLC analysis of antimicrobials

MON was extracted from the spiked cattle feed according to the AOAC method (Campbell and Nayeri, 2006). Briefly, an appropriate amount of the sample according to its concentration was placed in a 250 mL bottle and extracted using 100 mL of methanol/water solution (90:10, v/v) by shaking for 60 min at 225 rpm. Approximately 50 mL of the extract was centrifuged for 5 min at 3,000 rpm. After centrifugation, each sample was filtered through a 0.2 μm filter before SERS analysis. Meanwhile, for HPLC analysis, the sample was additionally diluted with 90% methanol extraction solution to the range of 0.5–4.5 μg/mL within the calibration curve of 0.25–5.0 μg/mL. The final dilution of each sample was then filtered through a 0.2 μm filter before injection into an HPLC system for analysis.

Likewise, the modified AOAC method (Sanchez and Campbell, 2008) was used for the extraction of DEC in beef cattle feed. Approximately 10 g of sample was extracted with 100 mL of 1% $CaCl_2.2H_2O$/methanol solution by shaking for 90 min at 220–250 rpm. At least 40 mL of the extract was then centrifuged for 5 min at 2,500 rpm. The supernatant solution after centrifugation was filtered through a 0.2 μm filter and subjected to the following SERS analysis while an aliquot of each sample was appropriately diluted with 1% $CaCl_2.2H_2O$/methanol solution and then added with H_2O to reach a desired concentration of DEC for HPLC analysis.

LAS spiked in the cattle feed was extracted based on the method proposed by Focht (2008). First, an appropriate weight of sample according was put in a 250 mL in Erlenmeyer flask and diluted with 0.5% acidified methanol solution according to its concentration. The sample is then placed into a preheated ultrasonic bath (40 ± 5 °C) and sonicated for 20 min, followed by shaking for 1 h. After centrifugation of each sample at 2,000 rpm for 10 min, an aliquot of the sample is directly mixed with AuNP for SERS analysis, or it was appropriately diluted to the desired volume with 0.5% acidified methanol (extracting solution) and filtered with a PVDF filter before injecting into HPLC system.

The predetermined volumes of an aliquot were injected into HPLC systems. Different operating conditions of the HPLC systems used for analysis of the three antimicrobials in the present work were summarized in Table 2. Other detailed parameters and analytical conditions employed for analysis of the selected antimicrobials were described in more detail in the aforementioned publications (Campbell and Nayeri,

Table 2
Operating conditions of HPLC systems used for determination of monensin (MON), decoquinate (DEC), and lasalocid sodium (LAS) in spiked cattle feeds.

HPLC conditions	MON	DEC	LAS
HPLC system	Waters 2695 (Waters, Milford, MA)	Agilent 1100 (Agilent Technol., Palo Alto, CA)	Agilent 1100 (Agilent Technol., Palo Alto, CA)
Analytical Column	Spherisorb 4.6 × 150 mm, C18	Waters Symmetry ® C18 (4.6 × 150 mm, 5 μm)	Waters Symmetry ® C18 (4.6 × 150 mm, 5 μm)
Reference standard solution (mg/kg)	0.25–5.0	0.15–6.0	1.0–5.0
Mobile phase	94:6 MeOH:H_20 with 0.1% CH_3COOH	82.5/17.5 MeOH: H_20 + 5.0 g $CaCH_2H_20$	CH_3COONH_4 buffer/ CH_3CN:15:85
Flow rate	0.8 mL/min	1.1 mL/min	1.3 mL/min
Detector	Waters 2487 UV/VIS, 520 nm	Fluorescence detector 266 nm excitation 394 nm emission	Fluorescence detector 315 nm excitation 418 nm emission
Injection volume	50 μL	10 μL	50 μL
Software	Empower	Chemstation	Chemstation

2006; Focht, 2008; Sanchez and Campbell, 2008).

2.4. Preparation of gold nanoparticles

Gold nanoparticles (AuNPs) for SERS measurements were prepared with minor modifications to the previous method (Bastús et al., 2011). In brief, sodium citrate solution (2.2 mM) in 150 mL of analytical grade water was placed into a three-necked round-bottomed flask and heated with vigorously stirring for 30 min. The flask was connected to a condenser to prevent the loss of the evaporated solution. Once the boiling of the solution initiated, $HAuCl_4$ (1 mL, 25 mM) was added to the flask. After the solution color was changed from yellow to pale pink, the size of negatively-charged gold nanoparticles appeared to be about 10 nm in diameter which served as Au seeds for subsequent AuNP synthesis. The synthesized Au seeds in the same flask were cooled to reach the temperature of the solution at around 90 °C. $HAuCl_4$ (1 mL, 25 mM) was subsequently added to the flask vessel. After 30 min, the same solution was added with $HAuCl_4$ (1 mL, 25 mM) once more. The solution (50 mL) was then extracted and diluted with water (53 mL) and sodium citrate (2 mL, 60 mM). The resulting solution was then utilized as a seed solution and again diluted with water (53 mL) and sodium citrate (2 mL, 60 mM). This process was repeated until gold nanoparticles grow to larger and desirable particle sizes (approx. 70 nm) (Fig. 1). During this process, homogeneous size and shape of AuNPs could be achieved by preventing the formation of secondary nucleation and stabilizing the particles via the reduction of $HAuCl_4$ by sodium citrate. Besides, the preparation of AuNPs was reproducible and the prepared particles had an appropriate size and shape to promote their plasmon-enhanced phenomena for SERS measurements.

Transmission electron microscopy (TEM) images of synthesized AuNPs were made with a JEOL 1200EX operating at 100 kV (JEOL Ltd., Tokyo, Japan) to examine the size and morphology of the nanoparticles at different stages of synthesis. Zetasizer Nano ZS ZEN3600 analyzer (Malvern Instrument Ltd, UK) was also used to evaluate the size distribution of AuNPs. The TEM image and particle size distribution results indicated a relatively narrow range of monodispersed nanoparticles with less than 100 nm particle size (Fig. 1) which could be achieved by effectively controlling manufacturing conditions, for example, temperature, pH, and seed particle concentrations. These controlled conditions for particle growth could contribute to the high stability of the AuNP solution to a greater extent because the kinetics of $HAuCl_4$ reduction and the nucleation rate is largely dependent on temperature and pH of the solution. Under these conditions, the electrostatic interactions cannot impair the particles' stability in solution. Based on the particle size distribution and the previous studies (Verma et al., 2014; Zhao et al., 2012), the zeta potential was estimated at around −35 eV (neutral condition) at which the electrostatic repulsion and stability of the nanoparticles were considered to be desirable and increased. These observations indicate the prepared AuNPs would be no aggregation in solution and could have appropriate optical properties suitable for SERS measurements. We compared the Raman peak intensity of MON, DEC, and LAS samples at the same concentration that had been analyzed during the study period. The SERS signal was reproducible yielding almost identical Raman peak intensity and profile for the specific region and wavelength of sample extracts for each antimicrobial. Thus, it appears that the synthesized AuNPs for the study were stable and reusable at least over periods up to 3 months and are comparable to the synthesized gold nanoparticles reported in other previous works (Kuncicky et al., 2005; Sanz-Ortiz et al., 2015; Tian et al., 2014).

2.5. SERS measurement

A mixture solution was prepared by gently mixing 10 μL sample extract with 30 μL AuNP solution and 3 μL 1% NaCl solution. After equilibrium for 2 min at room temperature, 30 μL of the mixture solution was transferred to the Al capsule in the well plate for SERS measurements in triplicate using Raman Spectroscopy (RamanStation 400F, PerkinElmer, Beaconsfield, Buckinghamshire, U.K.). Reference standard solutions at different antimicrobial concentrations used for HPLC analyses (Table 2) were also mixed with AuNP and 1% NaCl solutions for SERS measurement in the same way to compare the results between the spectroscopic and standard wet chemical methods. Naturally

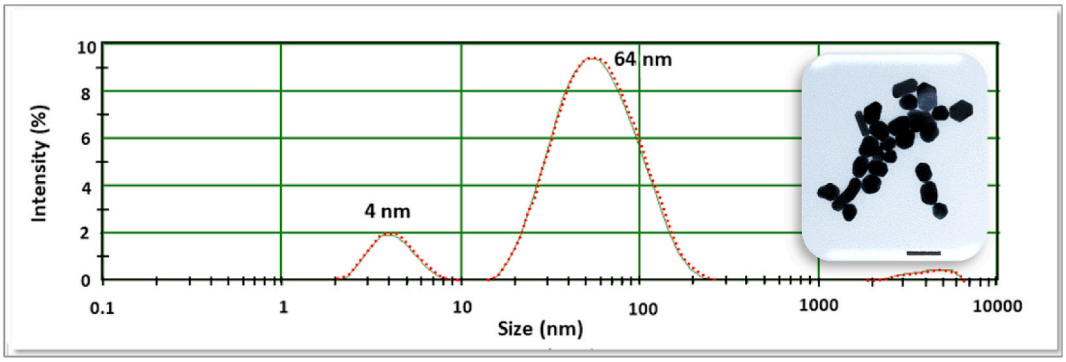

Fig. 1. Transmission electron microscopy (TEM) images and size distribution of gold nanoparticles (AuNPs) used for surface-enhanced Raman spectroscopy (SERS) measurement of antimicrobial spiked sample extracts. (For interpretation of the references to color in this figure legend, the reader is referred to the Web version of this article.)

contaminated feed samples at different concentrations were also analyzed as controls using Raman spectroscopy without employing AuNPs for comparison with SERS spectra. The Raman system interfaced with the software (Spectrum v. 6.3) for data acquisition and process consisted of a near-infrared laser source of 785 nm wavelength and a 256 x 1024 pixel charge-coupled device (CCD) detector. The laser power of 20 mW was delivered to the sample in the focus of 1.0-mm x 1.0-mm with exposure times of 15 s and 2 scans. The spectral data were recorded in the Raman shift range from 200 to 3,500 cm^{-1} at the spectral resolution of 4 cm^{-1}.

2.6. Preprocessing of spectra

The SERS spectrum of antimicrobial spiked feed sample extract was corrected for background at the time of its acquisition through a computational process using the embedded software (Spectrum v. 6.3). All spectra were further baseline-corrected and normalized in the specific Raman shift ranges to minimize unpredictable variation in Raman signal induced by subtle laboratory environmental changes and instrumental effects including monochromator drift with temperature, sample heating, sample radiation, photon flux incident, pixel-to-pixel variation, and temperature variation of detector elements (Bowie et al., 2000). These subtle changes may cause unpredictable artifacts including aliasing effect, increased noise level, wavenumber shift, broad bands, and hot pixels. The baseline-corrected and normalized spectra were also preprocessed by applying a 9-point Savitzky-Golay filtering function to obtain the first and second derivatives of the spectra. The deconvolution process was also carried out for the normalized spectra to improve the resolution of overlapped and unresolved bands. All preprocessed spectra were exported in ASCII format for further statistical analysis and the calculation procedures of the chemometric models for calibration and validation.

2.7. Development and validation of classification and quantification models

The preprocessed spectral data in ASCII format was used to develop the chemometric models for classification of the spiked feed samples based on the level of antimicrobial contamination using the two classification algorithms: linear discriminant analysis (LDA) and k-nearest neighbor (KNN). A linear discriminant analysis (LDA) assigned a sample into one of the antimicrobial concentration groups based on the Mahalanobis squared distance calculated using pooled covariance matrices (Johnson, 1998). That is, a sample is assigned to the group in which the samples are closest to the new sample. On contrary to LDA, the KNN algorithm is a nonparametric discrimination procedure. This chemometric algorithm is fundamentally dependent on the Mahalanobis distance between the pairs of the samples (Johnson, 1998). The procedure looks at the distances between a new sample and two or more other samples (i.e. k nearest neighbors) to assign the new sample to the group to which a majority of its neighbors are located. The selected chemometrics have been applied and proven to be suitable for in developing and validating the models on Raman spectra as well as explaining the relationship between target analytes and the acquired spectra, even the overlapped and low-quality spectra (Lee and Herrman, 2016; Lee et al., 2014). Multivariate statistical analyses including principal component analysis (PCA) and cluster analysis (CA) were also performed to see how well the spiked feed samples are classified into the predefined groups at different concentrations of antimicrobial. PCA is one of the commonly employed chemometric methods for screening complex multivariate data (Johnson, 1998; Lee et al., 2014). This algorithm uses a mathematical procedure to transform a set of correlated variables into a new set of uncorrelated variables (principal components). PCA is generally useful to classify test samples into several subgroups with similar properties. In this study, PCA used entire or selected characteristic Raman peaks to compute principal components of tested samples. CA is similar to discriminant analysis, but it classifies random samples whose origination is unknown beforehand (Johnson, 1998; Lee et al., 2014). For the study, CA was performed to classify large numbers of antimicrobial samples into subgroups with similar characteristics using Ward's minimum variance method option. As a result, all spiked samples were partitioned into 4 different subgroups and coded according to the level of antimicrobial in samples before the development of the classification models. The spectral data of 66 spiked samples were used as a training dataset to develop the calibration model while those of the validation samples ($n = 33$) independently prepared from different sample lots were employed to evaluate the performance of the calibration models. The developed models were compared to identify and determine the classification model with higher accuracy and better predictability based on two calculation values, a correct classification rate, and a false negative error.

The calibration models for antimicrobial quantification in animal feeds were developed based on the regression between the reference HPLC values and the preprocessed spectra by applying three chemometric methods including multiple linear regression (MLR), principal components regression (PCR), and partial least squares regression (PLSR). As seen from the development of classification models, the spectral data of training samples ($n = 66$) and independently prepared validation samples ($n = 33$) were used for developing and testing the models for each antimicrobial, respectively. The PCR and PLSR methods are a spectral decomposition technique. But the principle of regressing spectral data and the reference value is not identical between the two methods, yielding the different optimal number of extracted factors to explain the variance in the data (Lee et al., 2014). The predictability and suitability of PCR and PLSR models developed with different numbers of extracted factors were assessed based on coefficients of determination (r^2) and predicted residual sum of squares (PRESS) using a leave-one-out cross-validation method. Meanwhile, the calibration models developed from MLR determined the inclusion and the optimum number of wavelengths as input variables using stepwise regression and R^2 selection methods based on partial r^2 values, partial F-values, and PRESS. All chemometric models for antimicrobial quantification in animal feeds were externally validated using independently prepared, but similar samples. The sensitivity of the chemometric models was assessed with the external validation datasets based on the limit of detection (LOD) and the limit of quantitation (LOQ): $LOD = (|a| + 3S_a)/b$ and $LOQ = (|a| + 10S_a)/b$, respectively, where $|a|$ is the intercept on the y-axis, S_a represents the standard deviation for $|a|$, and b denotes the slope of the linear regression equation.

More details and relevant information about chemometric algorithms applied for the study can be found in previous studies (Delwiche and Hareland, 2004; Dowell et al., 2002; Lee et al., 2014; Johnson, 1998).

2.8. Statistical analysis

The statistical comparison between the model-predicted values and reference HPLC values was carried out through the ratio of the standard deviation of the reference data to the standard error of cross-validation (RPD), a paired sample t-test, and Pearson's correlation coefficient (r). SAS software (ver. 9.4, SAS Institute, Cary, NC) was mainly used to perform most statistical data analyses and development and validation procedures of the chemometric models for antimicrobial analysis.

3. Results and discussion

3.1. Spectral data processing and analysis

Selected feed samples were spiked with different concentration ranges of each antimicrobial, consequently showing various descriptive statistical values (Table 3). The descriptive statistics for each antimicrobial concentration were identical among the whole, training, and

validation datasets, except for kurtosis and skewness, which can be attributed to the different number of samples for each dataset. Although the present study mainly employed unnaturally contaminated samples and the sample size wasn't very large, the range of each antimicrobial concentration should cover the concentrations of most of the feed samples contaminated with antimicrobials found in the commercial market and feed industry. In fact, the maximum levels of antimicrobials legally permitted in the commercial products are mostly within the range of antimicrobial concentrations evaluated in the present study (Done et al., 2013). Besides, animal feeds produced in Texas which were collected and tested by our agency as a regulatory body for monitoring antimicrobial residues in the commercial feed products have rarely exceeded the maximal concentrations of antimicrobials spiked in samples used for the study. Therefore, the defined dataset may be sufficient and suitable for the development of the model for the analysis of antimicrobials in feeds, at least likely giving an idea and indication that the SERS technique would be applicable, beneficial, and promising compared to traditional wet chemical methods for a high throughput analysis.

The normalized average SERS spectra representing four different concentration groups of each antimicrobial are presented in Fig. 2. Raman shift regions in Fig. 2 showed spectral variations in SERS spectra by the concentration of antimicrobials in feed samples compared to standard Raman spectra although SERS intensity difference did not appear to be very significant, but depended on the type of antimicrobial. The presence of antimicrobials and their concentration in the spiked samples resulted in the visible spectral difference in SERS signal intensity in several spectral regions while similar spectral intensities were also observed in other spectral regions within each antimicrobial, probably due to the existence of identical constituents and chemical functional groups. The SERS signal intensity of antimicrobial spiked samples tended to be in proportion to the spiking level in some Raman shift regions regardless of the type of antimicrobial: 724–844 cm^{-1}, 1416–1504 cm^{-1}, and 1504–1688 cm^{-1} in MON; 632–804 cm^{-1}, 1048–1300 cm^{-1}, and 1352–1416 cm^{-1} in DEC; and 680–804 cm^{-1}, 1048–1356 cm^{-1}, and 1568–1700 cm^{-1} in LAS.

Such spectral differences resulting from the spiking level of antimicrobial are believed to be significant enough to develop the chemometric models with accuracy suitable for screening of contaminated feed samples. A similar quality spectral difference was also observed in the first and second derivative spectra of each antimicrobial (data not shown). SERS spectra of DEC sample extracts with a moderate difference in spiking level among the concentration groups exhibited a larger difference in Raman signal intensity among the groups compared to those of MON and LAS samples. This seems to imply that the spectral difference among different concentration groups is associated with the physiochemical and morphological properties of the antimicrobial molecule, rather than the level of spiking because DEC is known to have relatively smaller molecular weight and simpler molecular structure than MON and LAS (Zhang et al., 2012a).

Fig. 2 also clearly showed the characteristic peaks of the antimicrobial spiked sample extracts among different concentration groups and indicated that gold nanoparticles (AuNPs) could work for the detection and identification of the antimicrobials investigated in this study. However, as seen in Fig. 2, control samples measured without employing AuNPs showed very weak Raman intensity. Consequently, the Raman intensity difference among concentration groups of control samples was indistinctive and negligible. As mentioned above, the type of antimicrobial seemed to be more significantly associated with AuNPs' performance on detection property and limit, rather than the level of antimicrobial spiking. The aforementioned Raman shift regions showing a large difference in SERS signal intensity are believed closely associated with various chemical functional groups of antimicrobials and other constituents extracted from the animal feeds. The distinctive SERS peaks were observed at around 795, 1443, and 1604 cm^{-1} of MON extracts, 676, 736, and 1389 cm^{-1} of DEC extracts, and 788 and 1118 cm^{-1} of LAS extracts (Fig. 2). The intensity of these peaks was positively or negatively proportional to the concentration of antimicrobials up to the highest concentration of each antimicrobial. Meanwhile, other peaks in the given spectral regions associated with other constituents in the sample extract were not linearly proportional to an increase in antimicrobial concentration, showing low and insignificant correlations in later statistical analyses. The individual wavelengths with Raman peak intensity correlated with an antimicrobial concentration in the given regions exhibited a statistical significance with PCA factor loadings, regression coefficients of PLS models, and Pearson correlation coefficients.

An individual antimicrobial may require a uniquely designed SERS sensor which selectively functions well for the specific antimicrobial than other antimicrobials. In this study, AuNPs for SERS detection of antimicrobial analysis were not designed and modified for the single antimicrobial to induce a high binding affinity and physiochemical interaction on the metallic surface. However, as seen in Fig. 2, unmodified AuNPs seemed to have a strong and favorable interaction with a part of functional chemical groups of all three antimicrobials and yielded selectively enhanced Raman signals enough for the detection and characterization of the selected antimicrobials. No significant difference in the average spectra was also observed between reference standard solutions and spiked feed sample extracts for each antimicrobial. Specifically, strong SERS signals and unique characteristic peaks corresponding to some functional chemical groups of antimicrobials were not impaired at all by the presence of the interfering constituents and ions in the coextracts of one of most complex feed matrices. These findings and implications indicate an acceptable selectivity of the SERS sensor for the analysis of the selected antimicrobials in animal feed. In fact, it was considered that unmodified AuNPs would provide more benefits in terms of a practical approach than the synthesis of modified AuNPs because the preparation of the modified nanoparticles may require complex, expensive, and time-consuming steps. The complicated and costly synthesis steps could hinder the application of a rapid spectroscopic method for a routine screening method for a high volume of the regulatory samples. Even more exclusive and laborious efforts may be required when, as in this study, the synthesis of AuNPs for three different antimicrobials or simultaneous detection of multiple antimicrobial

Table 3
Selected descriptive statistics for feed samples spiked with MON, DEC, and LAS.

Antimicrobial	Dataset	Count, n	Mean, mg/kg	Median, mg/kg	Range, mg/kg	Kurtosis	Skewness
MON	Whole	99	14.6	12.5	0–50	2.15	1.48
	Training	66				2.44	1.52
	Validation	33				3.60	1.65
DEC	Whole	99	27.7	15.0	0–100	0.30	1.26
	Training	66				0.44	1.29
	Validation	33				0.97	1.40
LAS	Whole	99	43.9	30.0	0–150	0.47	1.17
	Training	66				0.62	1.20
	Validation	33				1.21	1.30

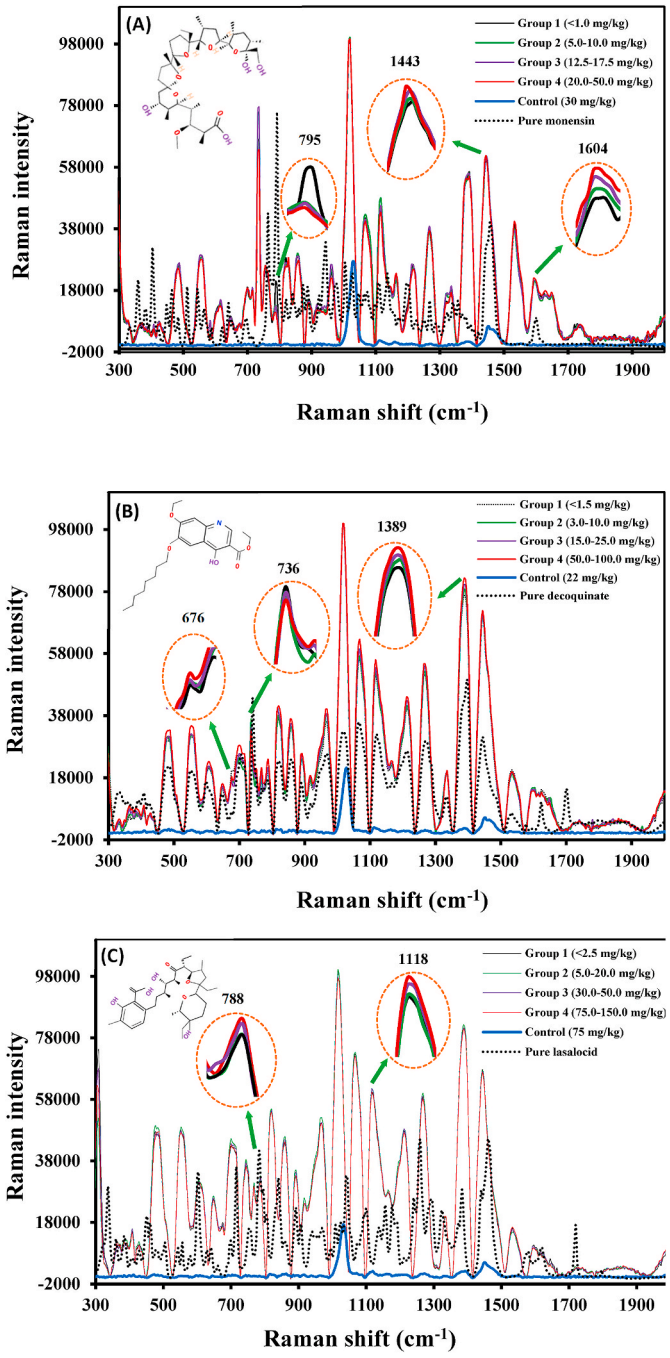

Fig. 2. Average SERS spectra of feed samples spiked with different levels of each antimicrobial concentrations and standard Raman spectra of control samples at specific concentrations and pure antimicrobials: (A) monensin (MON), (B) decoquinate (DEC), and (C) lasalocid (LAS).

residues need to be optimized. As mentioned earlier, extraction procedures employed for purification of MON, DEC, and LAS molecules were relatively simple and proved to be sufficiently effective for the removal of major interfering peaks and isolation of target analytes. This implies that neither extensive preparation steps nor a costly synthesis of modified AuNPs might be necessary for the situation when a high-throughput analysis and moderate selectivity are suitable and desirable. However, designing a SERS sensor capable of higher binding affinity and more favorable interaction with target antimicrobial molecules is certainly desirable and needs to be achieved for lower limits of detection and higher selectivity.

The major Raman peaks of interest were tentatively assigned to vibrational modes of antimicrobial molecules based on previous works (Picquart, 2000; Smith and Dent, 2005) and using a spectroscopy software (KnowItAll®, Bio-Rad, Hercules, CA). In MON, the prominent peaks at 795, 1443, and 1604 cm^{-1} can be attributed to C–C–O in-phase stretching, asymmetric CH_3 stretching, and aromatic ring stretching, respectively. Likewise, the Raman peaks at 676, 736, and 1389 cm^{-1} of DEC extracts are considered to correspond to C–C═O deformation, CC skeletal vibration, and CH rocking, respectively. The C–C–O in-phase stretching at 788 cm^{-1} and out-of-phase stretching at 1118 cm^{-1} also appeared to be largely influenced by the concentration of LAS in sample extracts.

As proposed in the previous studies, AuNPs are useful SERS substrates for the detection of trace chemical and biochemical hazards in food and feed, including antimicrobial residues because of a strong chemical interaction of antimicrobial molecules on the surface of the metallic particles. The identified characteristic peaks mentioned above were clear although the feed sample used for the study is considered a very complex matrix with significant amounts of protein, different types of carbohydrates, and other micronutrients which should be a major obstacle in SERS application for detection of a trace amount of antimicrobial residue in the extract. No significant interfering peaks due to other coextractants were observed, which can be attributed to the effective removal of other constituents after a few simple extraction steps including purification, filtration, and centrifugation. MON, DEC, and LAS have the chemical structure that facilitates the selective binding formation with AuNPs to promote the electromagnetic effect and thus enhance Raman scattering efficiency. The binding and electrostatic interaction between antimicrobial molecules and sodium citrate layer on AuNPs can lead to the aggregation of the particles to create SERS hot spots which are regions of strongly localized electromagnetic near-field responsible for highly sensitive SERS detection of the target analytes. The hot spots between adjacent AuNPs would produce a much stronger signal than the individual AuNP (Li et al., 2011). The MON, DEC, and LAS molecules have high hydrophilicity and ether groups which can facilitate interacting with the surfaces of AuNPs via hydrogen and ionic bonds (Luo et al., 2018).

These observations and implications indicate that SERS response is sensitive enough to measure variations induced by the concentration of the selected antimicrobials in the sample extracts. The interesting major peaks and fingerprint regions in the pure antimicrobial agent were consistently found in the corresponding spiked sample extracts. However, the location and intensity of the SERS peaks in the specific spectral regions were not identical between the two sample types, which could lead to Raman band assignments and data interpretation somewhat difficult and unclear for SERS spectra of the sample extract (Fig. 2). As mentioned above, such inconsistency in the spectra between the pure antimicrobial agent and spiked sample extract might be attributed to the fact that the SERS peaks of antimicrobial could be interfered with and contributed from multiple functional groups of other constituents extracted from the spiked feed samples. In addition to changes in the chemical and structural properties of antimicrobial molecules after extraction, the altered binding, chemical interaction, and orientation of functional chemical groups on the metallic surface could also induce some variations in the Raman peak intensity and sharpness (Lee and Herrman, 2016; Mandrile et al., 2018; Zhang et al., 2012a, 2012b). The orientation of antimicrobial molecules to the surface of AuNPs may vary due to the reversible physical interaction and covalent bonding of the molecules to the metallic surface (Olavarri'a-Fullerton et al., 2011). The consistency of the SERS signal could be influenced by the fitness of the antimicrobial molecule to the morphology of the SERS substrate and the distribution of nanoparticles. The imperfect homogeneous distribution of AuNPs may cause the inconsistent distribution of hot spots due to inconsistent reaction of antimicrobial molecules with the metallic surface, consequently affecting Raman scattering effect and signal intensity (Bastús et al., 2011; Lee and Herrman, 2016). The size of AuNPs

employed for the study was monodispersed and well-controlled. However, it was not quite optimized and might have needed to increase to move to closer to the excitation wavelength of the laser (785 nm) to maximize local electromagnetic enhancement and thus SERS signal for better spectral consistency and repeatability (Bastús et al., 2011; Amendola et al., 2017).

3.2. Development and validation of chemometric classification models

Chemometric models by applying *k*-nearest neighbor (KNN) and linear discriminant analysis (LDA) algorithms were developed to classify antimicrobial spiked samples into four sample groups at different antimicrobial concentrations using the Raman shift region of 400–1800 cm^{-1}. The classification accuracy results of the KNN models applied to the preprocessed spectral data of MON, DEC, and LAS are summarized in Table 4. The selected chemometric algorithms appear to be suitable for processing large spectral data in extracting more useful and valuable information from such complex data and explaining the relationship between Raman spectrum and antimicrobial concentration. The performance of KNN and LDA classification models was similar when the normalized spectral data used. However, only the KNN models are presented in Table 3 because they showed slightly better predictive accuracy and fewer prediction errors on the external validation samples than LDA models. Regardless of the type of antimicrobial, all classification models of the KNN and LDA models showed the correct classification rates of 100% for the resubstitution method that is in general considered to yield the underestimated misclassification rates (Johnson, 1998). In the KNN classification models, the classification accuracy of the models became stable and higher from the number of nearest neighbors with more than 2. For SERS spectra of all three antimicrobial samples, the KNN models developed with a training dataset showed excellent classification rates in the cross-validation method (100%) and model predictions (100%) on the independent validation dataset, except for the model for classification of DEC spiked samples in the concentration range of 50–100 mg/kg (Table 4). The misclassified DEC sample was incorrectly assigned to Group 2 that consisted of the samples with the concentrations close to that of the misclassified sample. It may be noteworthy that no KNN and even LDA models applied to validation datasets misclassified any samples contaminated with the selected antimicrobials as antimicrobial negative (false negative). No misclassification of antimicrobial positive samples using the SERS method is critical, which may imply that the SERS technique would be a promising and powerful tool for a high-throughput analysis for the rapid screening of antimicrobial contaminated samples. This should help manage the risk of humans and animals exposed to antimicrobial agents, thus improving food and feed safety in the supply chains.

The dendrogram of cluster analysis showed a clear separation of samples according to the type of antimicrobial when using the entire or selected feature wavelengths and the first few principal components with the higher eigenvalues. However, within each antimicrobial, the classification of antimicrobial spiked samples using hierarchical Ward's minimum variance method was not clearly configured by the group at different antimicrobial concentrations. Likewise, antimicrobial spiked samples were explicitly assigned to the predefined group according to the type of antimicrobial on the scatter plot created with the first two principal component scores. The results are in good agreement with the previous study reported by Omar et al.[29] In their study, near- and mid-infrared spectroscopic techniques successfully classified different feed additives containing the same or different coccidiostats as an active substance in principal component analysis (PCA) and partial least square-discriminant analysis (PLS-DA) models for training and validation datasets. They concluded that all ingredients of the feed additives could contribute to a high correct classification accuracy of the developed models for the products and active ingredients, which is similar to what is seen in the present study. However, as observed in cluster analysis, the samples within each antimicrobial were not precisely clustered to the different concentration groups. Meanwhile, the canonical discriminant scores derived from linear discriminant analysis on the selected wavelengths that were also used to build a scatter plot enabled us to differentiate among groups of antimicrobial spiked samples (Fig. 3). The scatter plot created by the first two canonical discriminant variables with higher discriminating power that is the combination of the original variables (feature wavelengths) effectively classified the antimicrobial contaminated samples into the predefined different groups. Although the pattern of the scatter plot is unique for each antimicrobial, the plot appeared to show the actual distance between the groups with keeping the samples within the same group closer together and grouping the samples with different antimicrobial concentrations and unique spectral properties remotely in the reduced, two-dimensional space. Such observations seem to be in a good agreement with the classification results of the chemometric classification models developed with SERS spectral data. As a result, no regions were found that showed the overlap among the groups in all the scatter plots by the principal components and canonical discriminant scores (Fig. 3). Regardless of the type of antimicrobial, the first two canonical variables were statistically significant ($p < 0.001$) and largely contributed to the discrimination among different concentration groups, explaining more than 95% of the total variation in normalized spectral data.

3.3. Development and validation of chemometric quantification models

Different chemometric methods including multiple linear regression

Table 4
Correct classification rates of antimicrobial contaminated groups at different concentrations based on KNN algorithm applied to the normalized spectral data[a].

Antimicrobial	Group (concentration, mg/kg)	Total no. of samples	Training sample		Validation sample		False negative error (%)[b]
			%	*n*	%	*n*	
MON	1 (0.0–1.0)	18	100.0	12	100.0	6	0.0
	2 (5.0–10.0)	27	100.0	21	100.0	6	0.0
	3 (12.5–17.5)	27	100.0	21	100.0	6	0.0
	4 (20.0–50.0)	27	100.0	21	100.0	6	0.0
DEC	1 (0.0–1.5)	18	100.0	12	100.0	6	0.0
	2 (3.0–10.0)	27	100.0	21	100.0	6	0.0
	3 (15.0–25.0)	27	100.0	21	100.0	6	0.0
	4 (50.0–100.0)	27	100.0	21	50.0	3	0.0
LAS	1 (0.0–2.5)	18	100.0	12	100.0	6	0.0
	2 (5.0–20.0)	27	100.0	21	100.0	6	0.0
	3 (30.0–50.0)	27	100.0	21	100.0	6	0.0
	4 (75.0–150.0)	27	100.0	21	100.0	6	0.0

[a] KNN, *K*-nearest neighbor.
[b] A false negative error (%) was calculated by dividing the number of misclassified contaminated samples as negative (Group 1) using the model by the total number of contaminated samples (Groups 2, 3, and 4).

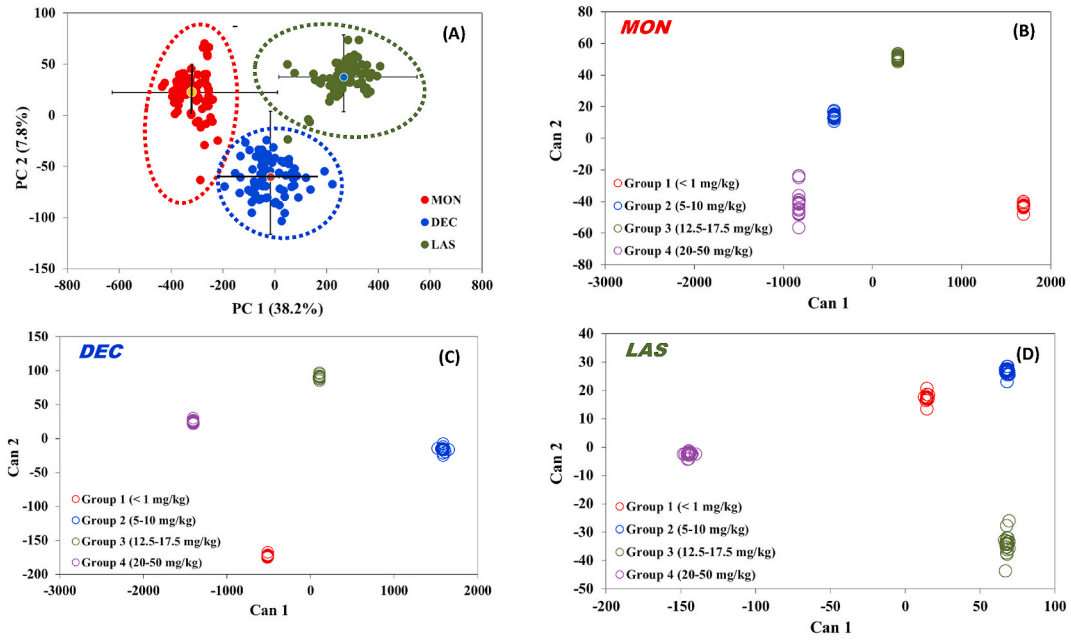

Fig. 3. The scatter plots crated with the first two principal component (PC) scores for the type of antimicrobial (A) and two canonical discriminant scores (CAN) for the different concentration groups within each antimicrobial: (B), monensin (MON), (C), decoquinate (DEC), and (D) lasalocid (LAS). Error bars represent 95% confidence intervals of the PC scores.

(MLR), partial least squares regression (PLSR), and principal component regression (PCR) for SERS spectral data at Raman spectral range of 400–1800 cm^{-1} were used to develop the calibration models to correlate Raman spectra with antimicrobial concentrations in reference standard solutions and spiked sample extracts. The applied chemometric techniques used the spectral regions and characteristic peaks highly correlated with the reference values and chemical features induced by an antimicrobial presence so that it may allow differentiating a subtle difference between contaminated and non-contaminated samples as well as contaminated samples for quantification of the target antimicrobials in actual samples. The relationships between actual concentrations of each antimicrobial and predicted values by the chemometric models on SERS spectral data are presented in Figs. 3 and 4 and Fig. S2–S4. The results of statistical analysis appeared to be largely influenced by the type of antimicrobial and the chemometric method.

Fig. 4 shows the relationships between actual concentrations of standard solutions for each antimicrobial and predicted values by MLR models built on SERS spectral data. The performance of MLR models was not significantly different among antimicrobials. MLR calibration models displayed high predictive accuracy, low error rate, and good regression quality, which appeared to be comparable to HPLC reference methods employed for the study in the range of low antimicrobial concentrations (Table 2). Other PLSR and PCR calibration models also gave equal predictability and satisfactory statistical results (data not shown). As seen in Fig. 4, MLR calibration models showed high r^2 values (0.989 for MON, 0.978 for DEC, and 0.967 for LAS) and low RMSEC values (0.247 mg/kg for MON, 0.326 mg/kg for DEC, and 0.311 for LAS). The slopes of all MLR models were in the range of 0.915–976, indicating the acceptable quality of the regression while the limit of detection (LOD) and the limit of quantitation (LOQ) were in the ranges of 0.381–0.506 mg/kg and 1.000–1.488 mg/kg, respectively. These observations seem to allow us to infer that the proposed spectroscopic method is as accurate as HPLC methods for standard solutions containing low concentrations of the selected antimicrobials.

However, the chemometric models developed on the SERS spectral of spiked sample extracts produced different statistical results depending on the type of antimicrobial and chemometric algorithm. Of chemometric quantification models for MON and DEC spiked sample extracts, MLR and PLSR models for SERS spectral data displayed good regression quality, high predictive accuracy, and low predictive error. However, the predictive accuracy and error rate of PCR models for MON and DEC were far less satisfactory compared to those of MLR and PLSR models. Likewise, in predicting LAS concentrations in spiked sample extracts for both training and validation datasets, the MLR and PLSR models performed much better than the PCR model. In the MLR model, the input variables (wavelengths) were selected through a stepwise regression variable selection and R^2 selection procedures. The selected wavelengths were further examined to remove any collinearity among the wavelengths and model overfitting problems as described in our previous study (Lee et al., 2014). All MLR models for the spectra could account for more than 85% of the variance in the spectral data (Fig. 5). The MLR models for the training datasets of antimicrobials yielded very high r^2 values of greater than 0.974 and acceptable error rates (RMSEC = 0.912–7.365 mg/kg). The validation datasets applying to the MLR calibration models produced slightly lower performance values, but still acceptable levels of predictive accuracy and error rates (r^2 = 0.856–0.932 and RMSEP = 3.877–18.234 mg/kg). Likewise, the MLR models for the training and validation datasets also displayed acceptable slopes of the linear regressions with good linearity in the ranges of 0.974–995 and 0.955–0.978, respectively. The selected wavelengths as input variables in the MLR models were certainly relevant to chemical functional groups of antimicrobial molecules and also presumably those of other molecules extracted from feed samples. These results indicate that the MLR models developed with SERS spectra could reasonably and accurately predict a certain level of antimicrobial concentration in the feed sample extract if further improvement and optimization are achieved in instrumentation and experimental conditions. However, as found in our previous works with SERS, the MLR modes were not very accurate in predicting lower concentrations in spiked sample extracts below or around the US Food and Drug Administration (FDA) Level of Concern for each antimicrobial (FDA, 2020). Such discrepancy between predicted and reference values at lower concentrations in the spiked sample extracts may be partially attributed to the absorption variation of antimicrobial molecules on or in the proximity of active sites (hot spots) on AuNPs due to competitive binding of other bioactive molecules in the extracts (Chen and Liu, 2012; Lee and Herrman, 2016; Wang et al.,

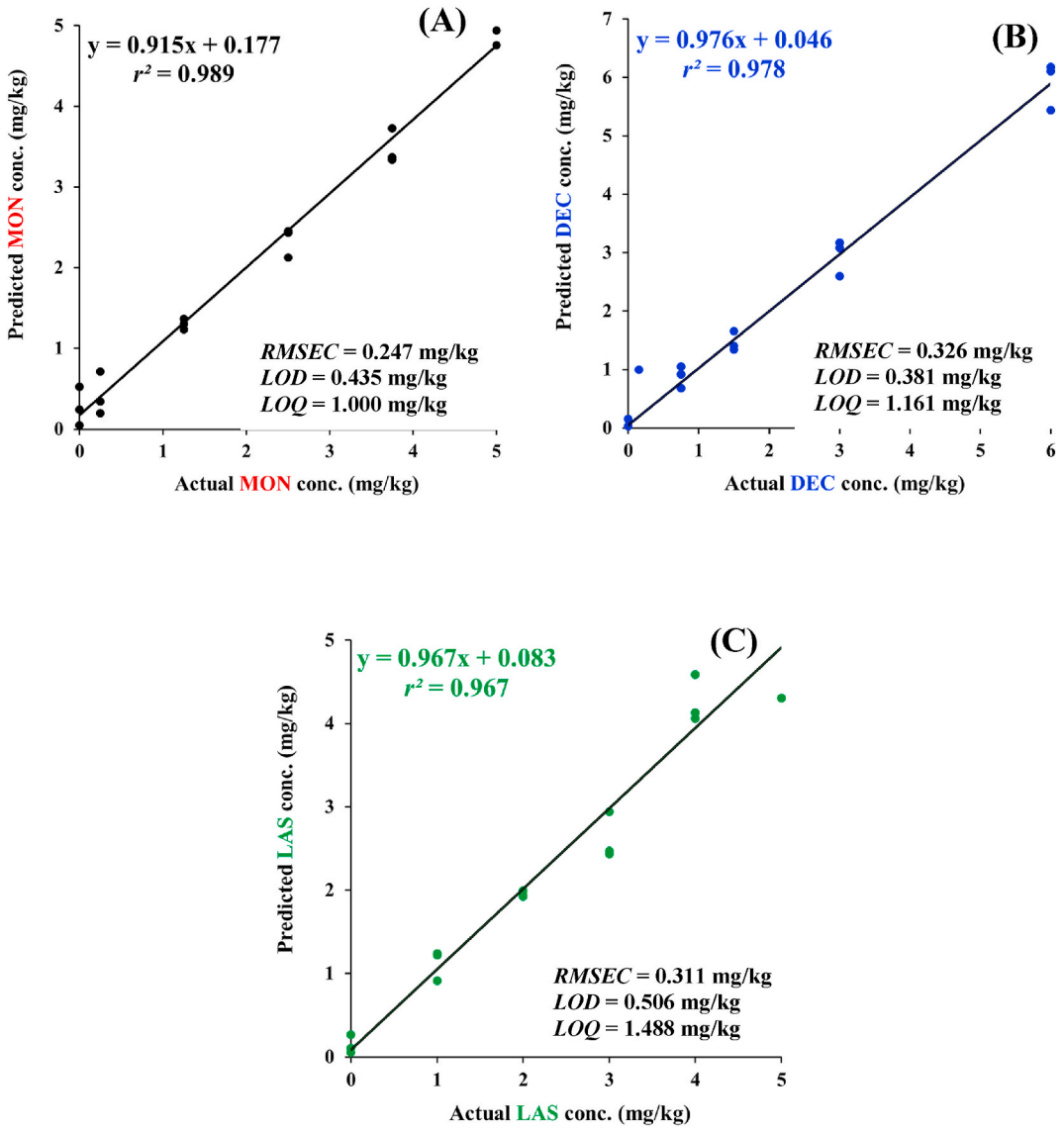

Fig. 4. Linear regression plots between predicted values by multiple linear regression (MLR) models built on SERS spectral data and HPLC reference values for (A) monensin (MON), (B) decoquinate (DEC), and (C) lasalocid (LAS) in standard solutions: LOD, limit of detection (mg/kg); LOQ, limit of quantitation (mg/kg); RMSEC, root-mean-square error of calibration (mg/kg).

2010). Besides, Raman laser penetration depth is limited, so that SERS may not be able to fully evaluate internal chemical compositions of a sample extract although such a limit is not imminent for high-concentration samples and standard solutions.

The PLSR, a quantitative regression algorithm, employed several factors to develop the calibration model that could extract almost all information on the entire range of SERS spectra in predicting antimicrobial concentration in a feed sample extract. The PLSR is a comparable regression algorithm to PCR, but it's more powerful and often produces more valid statistical inference (Lee et al., 2014; Osborne et al., 1993). The predicted residual error sum of squares (PRESS) was used to determine the optimum number of factors for the model based on the plot of PRESS and the number of factors as well as the p-value of the model residuals resulting from leave-one-out cross-validation method for the training dataset. More factors were needed for the PLSR model for LAS in spiked sample extracts whose quality was not as good as that of the other PLSR models for MON and DEC. As seen in the MLR models, the PLSR models for all antimicrobials yielded higher r^2 values (0.971–0.994) and lower error rates (RMSEC = 1.065–7.713 mg/kg) for the training datasets (Fig. 5). PLSR models applied to the validation datasets also produced comparable results to the MLR models regardless of the type of antimicrobial, overall resulting in high r^2 values (0.840–0.920) and low error rates (RMSEP = 4.068–18.474 mg/kg) (Fig. 5). The lower predictive accuracy and the higher error rate of the PLSR calibration models predicting the validation samples of LAS was somewhat unexpected. This may indicate that the resulting SERS spectra of LAS samples were less reproducible and probably acquired under inconsistent experimental conditions because the PLSR models are usually more vulnerable for small spectral variations to non-target analytes in the sample than other regression algorithms (Kim et al., 2008). The PCR models for all antimicrobials revealed much poorer predictive power and performance compared to the MLR and PLSR models, accounting for only 47.4–61.5% of the total variation in SERS spectra. The poor performance and inaccuracy of PCR models may be in part attributed to that PCR algorithm is a decomposition technique focusing on only the variance of the spectral data and is easily influenced by spectral similarity, low signal to noise ratio, poor repeatability of spectra, and interference of characteristic Raman bands from coextracts compared to other algorithms (Cramer, 1993; Osborne et al., 1993).

Although somewhat depending on chemometric method and the

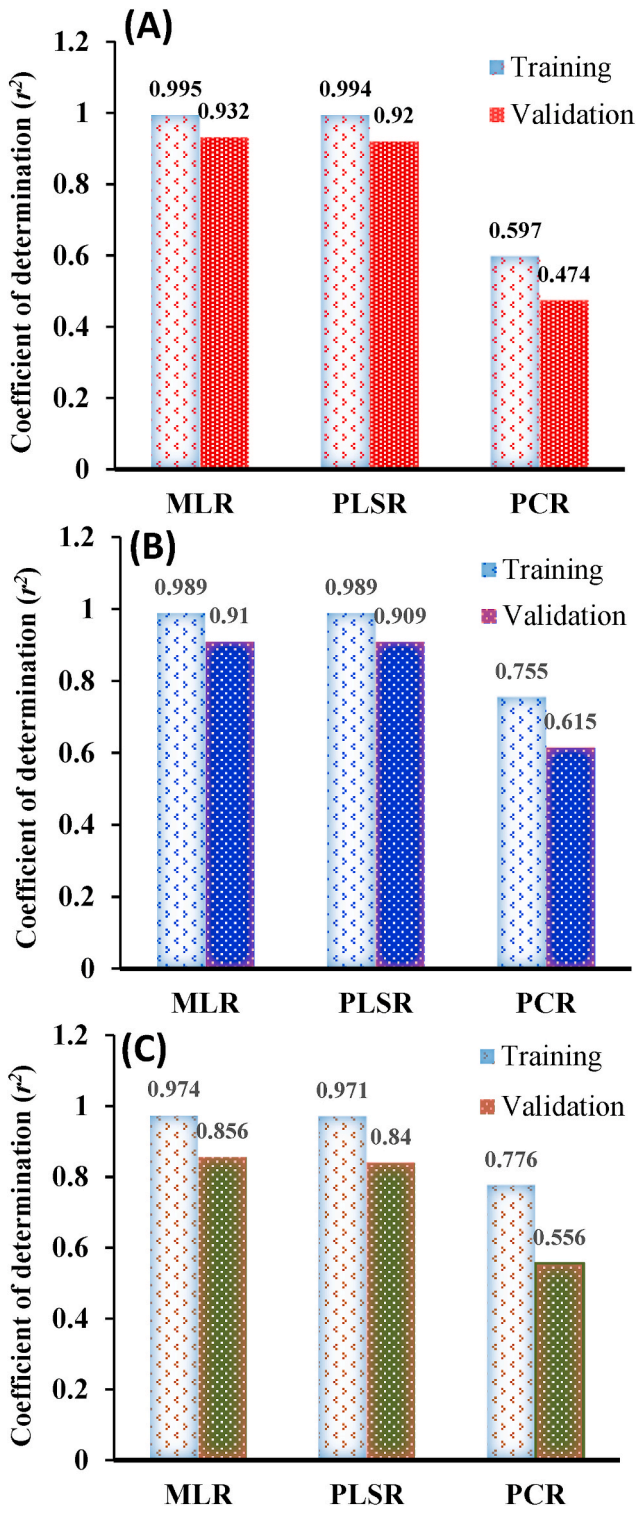

Fig. 5. Statistical results of multiple linear regression (MLR), partial least squares regression (PLSR), and principal component regression (PCR) models on SERS spectra for predicting concentrations of (A) monensin (MON), (B) decoquinate (DEC), and (C) lasalocid (LAS) in feed sample extracts: RMSEC, root-mean-square error of calibration (mg/kg); RMSEP, root mean-square error of prediction (mg/kg); LOD, limit of detection (mg/kg); LOQ, limit of quantitation (mg/kg); RPD, ratio of the standard deviation of the reference values to the standard error of cross-validation values; Std error, standard error of the mean difference between reference values and predicted values of SERS; r, Pearson correlation coefficient.

type of antimicrobial, the results of paired sample *t*-test for the validation datasets of all antimicrobials showed no statistically significant difference in antimicrobial concentrations in spiked sample extracts between the means of the reference HPLC method and SERS method ($p > 0.05$) (Fig. 5). Compared to antimicrobials in standard solutions (Fig. 4), the MLR and PLSR models displayed somewhat higher LOD and LOQ values in the ranges of 3.7–10.0 mg/kg and 10.8–26.3 mg/kg for MON and DEC (Fig. 5). Nevertheless, these findings indicate that the developed models might be still sensitive enough for screening or semi-quantitative analysis of antimicrobials in animal feeds. As would be expected, the standard error of paired differences between the model predicted and reference values showed the same trend observed in the other statistical results, that is, significantly lower in the MLR and PLSR models. Although poor or moderate correlations of PCR models were observed, the results of significance level (p-value) and correlation coefficient indicated the MLR and PLSR models yielded comparable values to HPLC values at antimicrobial levels in spiked sample extracts, implying a good agreement between SERS models and the reference methods. RPD (the standard error of cross-validation against the standard deviation of the reference values) values of the MLR models were 3.50 for MON and 3.21 for DEC. The PLSR model also showed a RPD value of 3.34 and 3.26 for MON and DEC, respectively. These high RPD values of greater than 3.0 indicated that such chemometric models may be effectively used for screening of antimicrobial contaminated feed or food samples. Although only a little study has been done to assess the utility of SERS for antimicrobial detection in feed samples, the current results of chemometric quantification models displaying high predictive accuracy and performance in determining antimicrobial concentration in standard solutions and spiked sample extracts are likely comparable to SERS methods for the analysis of various antimicrobials proposed in other previous studies (Table 5). The findings and inferences from the present research also clearly demonstrated SERS could be considered as an efficient and reliable analytical tool for antimicrobial quantification similar to other conventional or advanced spectroscopic methods when it comes to analytical sensitivity, cost-effectiveness, analytical convenience, and potential applicability for antimicrobial analysis.

4. Conclusion

In conclusion, the size-and shape-controlled gold nanoparticles (AuNPs) as a SERS agent with good binding affinity and chemical reaction with antimicrobial molecules proved to be applicable as a simple and efficient analytical tool alternative to conventional wet-chemical methods for rapid detection and screening of antimicrobial residues in regulatory feed samples with complex constituents. The SERS technique allowed direct and selective detection and characterization of selected antimicrobials and yielded discerning characteristic peaks proportional to the spiking level of the antimicrobials. The chemometric models for classification and quantification of antimicrobial levels exhibited high predictive accuracy and acceptable error rate with no misclassification of validation samples as antimicrobial negative below the level of regulatory concerns. The features and traits of SERS platforms coupled with chemometrics and a simple extraction procedure are worthwhile to be considered when it's required to develop a simple, rapid, and non-destructive spectroscopic method for routine analysis and real-time monitoring of antimicrobial contaminated samples at critical locations in the food or feed distribution systems. The methodology and implications from the study could be used as the basis for further researches on early screening of antimicrobial residues in various feed and food matrices. However, we think the size of AuNPs could have been better optimized and more dispersed to move the peak absorption wavelength of the particles close to the excitation wavelength of the laser to increase local electromagnetic enhancement for a higher quality of SERS signal. It's also worthwhile to further simplify a sample preparation procedure in combination with an effective approach of various chemometric methods in the future. For improvement of the applicability of AuNPs in

Table 5
Summary of SERS methods employed for analysis of different antimicrobials in previous studies.

Antimicrobial	Sample matrix or solution	SERS substrate	Selected characteristic peaks	Detection limit
Furadantin, & furaltadone (Xie et al., 2012)	Formamide, ethanol, & acetone	Au nanoparticles	1008 & 1162 cm^{-1}	5 mg/kg
Tetracycline (Li et al., 2011)	Milk	Ni/Au core-shell microparticles	1595 & 1320 cm^{-1}	0.1 mg/L (r^2 > 0.98)
Enrofloxacin, ciprofloxacin, & chloramphenicol (He et al., 2010)	Ethanol	Dendritic Ag nanosubstrates	1392 cm^{-1}	20 μg/L (r^2 > 0.98)
Furazolidone, & malachite green (Zhang et al., 2012a)	Fish	Klarite Substrate, & Q-SERS substrate	1332, 1394, 1606, &1615 cm^{-1}	0.2–1.0 mg/kg (r^2 > 0.92)
Leucomalachite green & malachite green (Zhang et al., 2012b)	Fish	Q-SERS substrate	432, 1170, 1360, & 1612 cm^{-1}	1–2 ng/g (r^2 > 0.733)
Chloramphenicol, & crystal violet (Lai et al., 2011)	Fish	Klarite Substrate	1170, 1350, 1588, & 1601 cm^{-1}	20–50 ng/mL (r^2 > 0.81)
Roxarsone & 4-arsanilic acid (OlavarríaFullerton et al., 2011)	Poultry feed additives	Silver/Polydimethylsiloxane Nanocomposites	792 cm^{-1}	
Methotrexate, aminopeni-cillanicacid, ampicillin-trihydrate, & penicillin G (Li et al., 2013)	Water	DisposableAg–graphenesensor	762, 1112, 1594, & 1000 cm^{-1}	0.3–0.8 nM
Penicillin G (Clarke et al., 2005)	Fermentation broths	Ag colloids	1005, 1220, 1380, 1475, &1606 cm^{-1}	50 mM

antimicrobial analysis, adsorption and interaction mechanism between target analytes and the surface on the particles needs to be better understood to design SERS substrates with higher selectivity and sensitivity. In the final analysis, SERS technique and SERS-based calibration models would be more practically applicable for antimicrobial analysis in the complex sample matrices only after some constraints and issues raised by the previous researches are solved including low-to-moderate repeatability and reproducibility of Raman spectra, expensive SERS substrate, unstable nanostructure, inappropriate sample preparation, and misapplication of chemometric methods. With further improvement and advancement in instrumentation and spectral data treatment, the SERS technique can certainly better serve as a more efficient and powerful tool for quality to help improve the safety of feed and food products supplied to animals and humans.

CRediT authorship contribution statement

Kyung-Min Lee: Conceptualization, Methodology, Validation, Data curation, Writing - original draft, Visualization, Supervision, Project administration, Formal analysis. **Danielle Yarbrough:** Software, Investigation. **Mena M. Kozman:** Software, Investigation. **Timothy J. Herrman:** Conceptualization, Writing - review & editing, Supervision, Project administration, Funding acquisition. **Jinhyuk Park:** Software, Investigation, Resources. **Rui Wang:** Software, Resources. **Dmitry Kurouski:** Resources, Writing - review & editing.

Declaration of competing interest

The authors declare that they have no known competing financial interests or personal relationships that could have appeared to influence the work reported in this paper.

Acknowledgements

The authors thank Mr. Rick Littleton at the Microscopy and Imaging Center (MIC) at Texas A&M University for assistance in obtaining the TEM images.

Appendix A. Supplementary data

Supplementary data to this article can be found online at https://doi.org/10.1016/j.fct.2020.111633.

References

Amendola, V., Pilot, R., Frasconi, M., Maragò, O.M., Iatì, M.A., 2017. Surface plasmon resonance in gold nanoparticles: a review. J. Phys. Condens. Matter 29 (20), 203002. https://iopscience.iop.org/article/10.1088/1361-648X/aa60f3/meta.

Athukorale, S., Leng, X., Xu, J.X., Perera, Y.R., Fitzkee, N.C., Zhang, D., 2019. Surface plasmon resonance, formation mechanism, and surface enhanced Raman spectroscopy of Ag+-stained gold nanoparticles. Front. Chem. 7 (2019), 27. https://www.frontiersin.org/articles/10.3389/fchem.2019.00027/full.

Bacanli, M., Başaran, N., 2019. Importance of antibiotic residues in animal food. Food Chem. Toxicol. 125, 462–466. https://www.sciencedirect.com/science/article/pii/S0278691519300456.

Bastús, N.G., Comenge, J., Puntes, V., 2011. Kinetically controlled seeded growth synthesis of citrate-stabilized gold nanoparticles of up to 200 nm: size focusing versus Ostwald ripening. Langmuir 27 (17), 11098–11105. https://pubs.acs.org/doi/abs/10.1021/la201938u.

Benito-Peña, E., Urraca, J., Moreno-Bondi, M., 2009. Quantitative determination of penicillin V and amoxicillin in feed samples by pressurised liquid extraction and liquid chromatography with ultraviolet detection. J. Pharmaceut. Biomed. Anal. 49 (2), 289–294. https://www.sciencedirect.com/science/article/pii/S0731708508006183.

Bigall, N.C., Härtling, T., Klose, M., Simon, P., Eng, L.M., Eychmüller, A., 2008. Monodisperse platinum nanospheres with adjustable diameters from 10 to 100 nm: synthesis and distinct optical properties. Nano Lett. 8 (12), 4588–4592. https://pubs.acs.org/doi/abs/10.1021/nl802901t.

Boscher, A., Guignard, C., Pellet, T., Hoffmann, L., Bohn, T., 2010. Development of a multi-class method for the quantification of veterinary drug residues in feedingstuffs by liquid chromatography-tandem mass spectrometry. J. Chromatogr. A 1217 (41), 6394–6404. https://www.sciencedirect.com/science/article/pii/S0021967310010769.

Bowie, B.T., Chase, D.B., Griffiths, P.R., 2000. Factors affecting the performance of bench-top Raman spectrometers. Part I: instrumental effects. Appl. Spectrosc. 54 (5), 164A–173A. https://journals.sagepub.com/doi/pdf/10.1366/0003702001949924.

Campbell, H., Nayeri, G., 2006. Determination of monensin, narasin, and salinomycin in mineral premixes, supplements, and animal feeds by liquid chromatography and post-column derivatization: collaborative study. J. AOAC Int. 89 (5), 1229–1242. http://lib3.dss.go.th/fulltext/E_content/1060-3271/AOAC%20Vol.%2089,%20Iss.%205.pdf.

Chattopadhyay, A., Komath, S.S., Raman, B., 1992. Aggregation of lasalocid A in membranes: a fluorescence study. Biochim. Biophys. Acta Biomembr. 1104 (1), 147–150. https://www.sciencedirect.com/science/article/pii/000527369290143A.

Chen, L.M., Liu, Y.N., 2012. Ag-nanoparticle-modified single Ag nanowire for detection of melamine by surface-enhanced Raman spectroscopy. J. Raman Spectrosc. 43 (8), 986–991. https://onlinelibrary.wiley.com/doi/full/10.1002/jrs.3137.

Chen, X., Lin, M., Sun, L., Xu, T., Lai, K., Huang, M., Lin, H., 2019. Detection and quantification of carbendazim in Oolong tea by surface-enhanced Raman spectroscopy and gold nanoparticle substrates. Food Chem. 293, 271–277, 2019. https://www.sciencedirect.com/science/article/pii/S0308814619307496.

Chen, Z., Yongyu, L., Yankun, P., Tianfeng, X., 2015. Detection of chlorpyrifos in apples using gold nanoparticles based on surface enhanced Raman spectroscopy. Int. J. Agric. Biol. Eng. 8 (5), 113–120. http://www.ijabe.org/index.php/ijabe/article/view/1771.

Clarke, L., Fodey, T.L., Crooks, S.R., Moloney, M., O'Mahony, J., Delahaut, P., O'Kennedy, R., Danaher, M., 2014. A review of coccidiostats and the analysis of their residues in meat and other food. Meat Sci. 97 (3), 358–374. https://www.sciencedirect.com/science/article/pii/S0309174014000059.

Clarke, S.J., Littleford, R.E., Smith, W.E., Goodacre, R., 2005. Rapid monitoring of antibiotics using Raman and surface enhanced Raman spectroscopy. Analyst 130 (7), 1019–1026. https://pubs.rsc.org/en/content/articlehtml/2005/an/b502540k.

Compagnini, G., Galati, C., Pignataro, S., 1999. Distance dependence of surface enhanced Raman scattering probed by alkanethiol self-assembled monolayers. Phys. Chem. Chem. Phys. 1 (9), 2351–2353. https://pubs.rsc.org/–/content/articlehtml/1999/cp/a901034c.

Craig, A.P., Franca, A.S., Irudayaraj, J., 2013. Surface-enhanced Raman spectroscopy applied to food safety. Annu Rev Food SciTech 4, 369–380. https://www.annualreviews.org/doi/abs/10.1146/annurev-food-022811-101227.

Cramer, R.D., 1993. Partial least squares (PLS): its strengths and limitations. Perspect. Drug Discov. Des. 1 (2), 269–278. https://link.springer.com/article/10.1007/BF02174528.

Delwiche, S.R., Hareland, G.A., 2004. Detection of scab-damaged hard red spring wheat kernels by near-infrared reflectance. Cereal Chem. 81 (5), 643–649. https://onlinelibrary.wiley.com/doi/abs/10.1094/CCHEM.2004.81.5.643.

Di Fabrizio, E., Schlücker, S., Wenger, J., Regmi, R., Rigneault, H., Calafiore, G., West, M., Cabrini, S., Fleischer, M., Van Hulst, N.F., Garcia-Parajo, M.F., 2016. Roadmap on biosensing and photonics with advanced nano-optical methods. J. Optic. 18 (6), 063003. https://iopscience.iop.org/article/10.1088/2040-8978/18/6/063003/meta.

Dorne, J.L., Fernández-Cruz, M.L., Bertelsen, U., Renshaw, D.W., Peltonen, K., Anadon, A., Feil, A., Sanders, P., Wester, P., Fink-Gremmels, J., 2013. Risk assessment of coccidostatics during feed cross-contamination: animal and human health aspects. Toxicol. Appl. Pharmacol. 270 (3), 196–208. https://www.sciencedirect.com/science/article/pii/S0041008X10004795.

Dowell, F.E., Pearson, T.C., Maghirang, E.B., Xie, F., Wicklow, D.T., 2002. Reflectance and transmittance spectroscopy applied to detecting fumonisin in single corn kernels infected with *Fusarium verticillioides*. Cereal Chem. 79 (2), 222–226. https://onlinelibrary.wiley.com/doi/abs/10.1094/CCHEM.2002.79.2.222.

Dowling, L., 1992. Ionophore toxicity in chickens: a review of pathology and diagnosis. Avian Pathol. 21 (3), 355–368. https://www.tandfonline.com/doi/abs/10.1080/03079459208418854.

Fan, M., Andrade, G.F., Brolo, A.G., 2011. A review on the fabrication of substrates for surface enhanced Raman spectroscopy and their applications in analytical chemistry. Anal. Chim. Acta 693 (1–2), 7–25. https://www.sciencedirect.com/science/article/pii/S0003267011003151.

FDA, 2020. Code of federal regulations, title 21-foods and drugs. Part 558 – new animal drugs for use in animal feeds. https://www.ecfr.gov/cgi-bin/text-idx?SID=feebc53a16a8c4 db2788e0dd98d0b6af&mc =true&node=pt21.6.558&rgn=div 5 (accessed 26 Feb 2020).

Feng, S., Hu, Y., Ma, L., Lu, X., 2017. Development of molecularly imprinted polymers-surface-enhanced Raman spectroscopy/colorimetric dual sensor for determination of chlorpyrifos in apple juice. Sens. Actuators, B 241, 750–757, 2017. https://www.sciencedirect.com/science/article/pii/S0925400516317610.

Focht, C., 2008. Determination of lasalocid sodium in animal feeds and premixes by reversed-phase liquid chromatography: collaborative study. J. AOAC Int. 91 (3), 479–488. http://lib3.dss.go.th/fulltext/E_content/1060-3271/2008v.91n.3.pdf.

García-Campaña, A.M., Gámiz-Gracia, L., Lara, F.J., del Olmo Iruela, M., Cruces-Blanco, C., 2009. Applications of capillary electrophoresis to the determination of antibiotics in food and environmental samples. Anal. Bioanal. Chem. 395 (4), 967–986. https://link.springer.com/article/10.1007/s00216-009-2867-9.

Harris, J., Russell, C.L., Wilkins, J.G., 1998. The characterisation of polyether ionophore veterinary drugs by HPLC-electrospray MS. Analyst 123 (12), 2625–2628. https://pubs.rsc.org/en/content/articlehtml/1998/an/a805112g.

Haynes, C.L., McFarland, A.D., Van Duyne, R.P., 2005. Surface-enhanced Raman spectroscopy. Anal. Chem. 77, 338A–346A. https://pubs.acs.org/doi/abs/10.1021/ac053456d.

He, L., Lin, M., Li, H., Kim, N.J., 2010. Surface-enhanced Raman spectroscopy coupled with dendritic silver nanosubstrate for detection of restricted antibiotics. J. Raman Spectrosc. 41 (7), 739–744. https://onlinelibrary.wiley.com/doi/full/10.1002/jrs.2505.

Hong, J., Kawashima, A., Hamada, N., 2017. A simple fabrication of plasmonic surface-enhanced Raman scattering (SERS) substrate for pesticide analysis via the immobilization of gold nanoparticles on UF membrane. Appl. Surf. Sci. 407, 440–446, 2017. https://www.sciencedirect.com/science/article/pii/S0169433217306050.

Jahn, M., Patze, S., Hidi, I.J., Knipper, R., Radu, A.I., Mühlig, A., Yüksel, S., Peksa, V., Weber, K., Mayerhöfer, T., Cialla-May, D., 2016. Plasmonic nanostructures for surface enhanced spectroscopic methods. Analyst 141 (3), 756–793. https://pubs.rsc.org/en/content/articlehtml/2016/an/c5an02057c.

Johnson, D.E., 1998. Discriminant analysis. In: Johnson, D.E. (Ed.), Applied Multivariate Methods for Data Analyst. Duxbury Press, Pacific Grove, CA, pp. 217–285.

Joshi, G.K., White, S.L., Johnson, M.A., Sardar, R., Jain, P.K., 2016. Ultrashort, angstrom-scale decay of surface-enhanced Raman scattering at hot spots. J. Phys. Chem. C 120 (43), 24973–24981. https://pubs.acs.org/doi/abs/10.1021/acs.jpcc.6b08242.

Kim, J., Hwang, J., Chung, H., 2008. Comparison of near-infrared and Raman spectroscopy for on-line monitoring of etchant solutions directly through a Teflon tube. Anal. Chim. Acta 629 (1–2), 119–127. https://www.sciencedirect.com/science/article/pii/S000326700801653X.

Kuncicky, D.M., Christesen, S.D., Velev, O.D., 2005. Role of the micro-and nanostructure in the performance of surface-enhanced Raman scattering substrates assembled from gold nanoparticles. Appl. Spectrosc. 59 (4), 401–409. https://journals.sagepub.com/doi/abs/10.1366/0003702053641559.

Kurittu, J., Lonnberg, S., Virta, M., Karp, M., 2000. A group-specific microbiological test for the detection of tetracycline residues in raw milk. J. Agric. Food Chem. 48 (8), 3372–3377. https://pubs.acs.org/doi/abs/10.1021/jf9911794.

Lai, K., Zhang, Y., Du, R., Zhai, F., Rasco, B.A., Huang, Y., 2011. Determination of chloramphenicol and crystal violet with surface enhanced Raman spectroscopy. Sens Instrum Food Qual Saf 5 (1), 19–24. https://link.springer.com/article/10.1007/s11694-011-9106-8.

Lee, K.M., Herrman, T.J., 2016. Determination and prediction of fumonisin contamination in maize by surface–enhanced Raman spectroscopy (SERS). Food Bioprocess Technol. 9 (4), 588–603. https://link.springer.com/article/10.1007/s11947-015-1654-1.

Lee, K.M., Herrman, T.J., Lingenfelser, J., Jackson, D.S., 2005. Classification and prediction of maize hardness-associated properties using multivariate statistical analyses. J. Cereal. Sci. 41 (1), 85–93. https://www.sciencedirect.com/science/article/pii/S0733521004001055.

Lee, K.M., Herrman, T.J., Yun, U., 2014. Application of Raman spectroscopy for qualitative and quantitative analysis of aflatoxins in ground maize samples. J. Cereal. Sci. 59 (1), 70–78. https://www.sciencedirect.com/science/article/pii/S0733521013001653.

Li, C., Huang, Y., Lai, K., Rasco, B.A., Fan, Y., 2016. Analysis of trace methylene blue in fish muscles using ultra-sensitive surface-enhanced Raman spectroscopy. Food Contr. 65, 99–105, 2016. https://www.sciencedirect.com/science/article/pii/S0956713516300184.

Li, D., Lv, D.Y., Zhu, Q.X., Li, H., Chen, H., Wu, M.M., Chai, Y.F., Lu, F., 2017. Chromatographic separation and detection of contaminants from whole milk powder using a chitosan-modified silver nanoparticles surface-enhanced Raman scattering device. Food Chem. 224, 382–389, 2017. https://www.sciencedirect.com/science/article/pii/S0308814616320519.

Li, R., Zhang, H., Chen, Q.W., Yan, N., Wang, H., 2011. Improved surface-enhanced Raman scattering on micro-scale Au hollow spheres: synthesis and application in detecting tetracycline. Analyst 136 (12), 2527–2532. https://pubs.rsc.org/en/content/articlehtml/2011/an/c1an15195a.

Li, Y.T., Qu, L.L., Li, D.W., Song, Q.X., Fathi, F., Long, Y.T., 2013. Rapid and sensitive in-situ detection of polar antibiotics in water using a disposable Ag–graphene sensor based on electrophoretic preconcentration and surface-enhanced Raman spectroscopy. Biosens. Bioelectron. 43, 94–100. https://www.sciencedirect.com/science/article/pii/S09565663 12008573.

Lombardi, J.R., Birke, R.L., 2009. A unified view of surface-enhanced Raman scattering. Acc. Chem. Res. 42 (6), 734–742. https://pubs.acs.org/doi/abs/10.1021/ar800249y.

Luo, H., Wang, X., Huang, Y., Lai, K., Rasco, B.A., Fan, Y., 2018. Rapid and sensitive surface-enhanced Raman spectroscopy (SERS) method combined with gold nanoparticles for determination of paraquat in apple juice. J. Sci. Food Agric. 98 (10), 3892–3898. https://onlinelibrary.wiley.com/doi/full/10.1002/jsfa.8906.

Mandrile, L., Giovannozzi, A.M., Durbiano, F., Martra, G., Rossi, A.M., 2018. Rapid and sensitive detection of pyrimethanil residues on pome fruits by Surface Enhanced Raman Scattering. Food Chem. 244, 16–24, 2018. https://www.sciencedirect.com/science/article/pii/S0308814617316321.

Matabudul, D.K., Lumley, I.D., Points, J.S., 2002. The determination of 5 anticoccidial drugs (nicarbazin, lasalocid, monensin, salinomycin and narasin) in animal livers and eggs by liquid chromatography linked with tandem mass spectrometry (LC-MS-MS). Analyst 127 (6), 760–768. https://pubs.rsc.org/en/content/articlehtml/2002/an/b200872f.

Matsuoka, T., Novilla, M.N., Thomson, T.D., Donoho, A.L., 1996. Review of monensin toxicosis in horses. J. Equine Vet. Sci. 16 (1), 8–15. https://www.sciencedirect.com/science/article/pii/S0737080696800591.

Moros, J., Garrigues, S., de la Guardia, M., 2010. Vibrational spectroscopy provides a green tool for multi-component analysis. TrAC Trends Anal. Chem. (Reference Ed.) 29 (7), 578–591. https://www.sciencedirect.com/science/article/pii/S0165993610000361.

Mortier, L., Daeseleire, E., Peteghem, C.V., 2005. Determination of the ionophoric coccidiostats narasin, monensin, lasalocid and salinomycin in eggs by liquid chromatography/tandem mass spectrometry. Rapid Commun. Mass Spectrom.: An International Journal Devoted to the Rapid Dissemination of Up-to-the-Minute Research in Mass Spectrometry 19 (4), 533–539. https://onlinelibrary.wiley.com/doi/full/10.1002/rcm.1819.

Moskovits, M., 2005. Surface-enhanced Raman spectroscopy: a brief retrospective. J. Raman Spectrosc. 36 (6-7), 485–496. https://onlinelibrary.wiley.com/doi/abs/10.1002/jrs.1362.

Oehme, F.W., Pickrell, J.A., 1999. An analysis of the chronic oral toxicity of polyether ionophore antibiotics in animals. Vet. Hum. Toxicol. 41 (4), 251–257. https://europepmc.org/article/med/10434384.

OlavarríaFullerton, J., Wells, S., Ortiz-Rivera, W., Sepaniak, M.J., De Jesus, M.A., 2011. Surface-enhanced Raman scattering (SERS) characterization of trace organoarsenic antimicrobials using silver/polydimethylsiloxane nanocomposites. Appl. Spectrosc. 65 (4), 423–428. https://www.osapublishing.org/as/abstract.cfm?uri=as-65-4-423.

Omar, J., Boix, A., von Holst, C., 2015. Differentiation of coccidiostats-containing feed additives by mid and near infrared microscopy. Food Addit. Contam. 32 (9), 1464–1474. https://www.tandfonline.com/doi/full/10.1080/19440049.2015.1075177.

Osborne, B.G., Fearn, T., Hindle, P.H., 1993. Practical NIR spectroscopy with applications in food and beverage analysis. In: Osborne, B.G., Fearn, T., Hindle, P.H. (Eds.), Near Infrared Calibration II. Longman Scientific & Technical., Harlow, UK, pp. 121–144.

Pan, T.T., Sun, D.W., Pu, H., Wei, Q., 2018. Simple approach for the rapid detection of alternariol in pear fruit by surface-enhanced Raman scattering with pyridine-

modified silver nanoparticles. J. Agric. Food Chem. 66 (9), 2180–2187. https://pubs.acs.org/doi/abs/10.1021/acs.jafc. 7b05664.

Picquart, M., 2000. Interaction of antibiotics Lasalocid and Monensin with model membranes evidenced by Raman spectroscopy and FT-IR. Rev. Mexic. Fisica 46 (2), 166–173. https://inis.iaea.org/search/search.aspx?orig_q=RN:31025175.

Plieth, W., Dietz, H., Anders, A., Sandmann, G., Meixner, A., Weber, M., Kneppe, H., 2005. Electrochemical preparation of silver and gold nanoparticles: characterization by confocal and surface enhanced Raman microscopy. Surf. Sci. 597 (1–3), 119–126. https://www.sciencedirect.com/science/article/pii/S0039602805007922.

Roggo, Y., Chalus, P., Maurer, L., Lema-Martinez, C., Edmond, A., Jent, N., 2007. A review of near infrared spectroscopy and chemometrics in pharmaceutical technologies. J. Pharmaceut. Biomed. Anal. 44 (3), 683–700. https://www.sciencedirect.com/science/article/pii/S0731708507001884.

Sanchez, A.A., Campbell, H.M., 2008. Determination of decoquinate in animal feeds by liquid chromatography: collaborative study. J. AOAC Int. 91 (4), 685–693. http://lib3.dss.go.th/fulltext/e_content/1060-3271/2008v.91n.4.pdf.

Sanz-Ortiz, M.N., Sentosun, K., Bals, S., Liz-Marzán, L.M., 2015. Templated growth of surface enhanced Raman scattering-active branched gold nanoparticles within radial mesoporous silica shells. ACS Nano 9 (10), 10489–10497. https://pubs.acs.org/doi/abs/10.1021/acsnano.5b04744.

Separovic, L., de Godoy Bertanha, M.L., Saviano, A.M., Lourenço, F.R., Conformity, 2019. Decisions based on measurement uncertainty—a case study applied to agar diffusion microbiological assay. J Pharm Innovation 1–6, 2019. https://link.springer.com/article/10.1007/s12247-019-09374-8.

Simoncelli, S., Roller, E.M., Urban, P., Schreiber, R., Turberfield, A.J., Liedl, T., Lohmüller, T., 2016. Quantitative single-molecule surface-enhanced Raman scattering by optothermal tuning of DNA origami-assembled plasmonic nanoantennas. ACS Nano 10 (11), 9809–9815. https://pubs.acs.org/doi/abs/10.1021/acsnano.6b05276.

Smith, E., Dent, G., 2005. Introduction, basic theory and principles. In: Smith, E., Dent, G. (Eds.), Modern Raman Spectroscopy-A Practical Approach. West Sussex, West Sussex, UK, pp. 1–21.

Tian, F., Bonnier, F., Casey, A., Shanahan, A.E., Byrne, H.J., 2014. Surface enhanced Raman scattering with gold nanoparticles: effect of particle shape. Anal. Methods 6 (22), 9116–9123. https://pubs.rsc.org/en/content/articlehtml/2014/ay/c4ay02112f.

Verma, H.N., Singh, P., Chavan, R.M., 2014. Gold nanoparticle: synthesis and characterization. Vet. World 7 (2), 72–77. https://search.proquest.com/docview/1503119256?pq-origsite= gscholar.

Wang, Y., Lee, K., Irudayaraj, J., 2010. Silver nanosphere SERS probes for sensitive identification of pathogens. J. Phys. Chem. C 114 (39), 16122–16128. https://pubs.acs.org/doi/abs/10.1021/jp1015406.

Weber, C.C., Link, N., Fux, C., Zisch, A.H., Weber, W., Fussenegger, M., 2005. Broad-spectrum protein biosensors for class-specific detection of antibiotics. Biotechnol. Bioeng. 89 (1), 9–17. https://onlinelibrary.wiley.com/doi/abs/10.1002/bit.20224.

Wu, Y.X., Liang, P., Dong, Q.M., Bai, Y., Yu, Z., Huang, J., Zhong, Y., Dai, Y.C., Ni, D., Shu, H.B., Pittman Jr., C.U., 2017. Design of a silver nanoparticle for sensitive surface enhanced Raman spectroscopy detection of carmine dye. Food Chem. 237, 974–980, 2017. https://www.sciencedirect.com/science/article/pii/S0308814617310397.

Xie, Y., Zhu, X., Sun, Y., Wang, H., Qian, H., Yao, W., 2012. Rapid detection method for nitrofuran antibiotic residues by surface-enhanced Raman Spectroscopy. Eur. Food Res. Technol. 235 (3), 555–561. https://link.springer.com/article/10.1007/s00217-012-1752-5.

Yan, M., She, Y., Cao, X., Ma, J., Chen, G., Hong, S., Shao, Y., Abd El-Aty, A.M., Wang, M., Wang, J., 2019. A molecularly imprinted polymer with integrated gold nanoparticles for surface enhanced Raman scattering based detection of the triazine herbicides, prometryn and simetryn. Microchim. Acta 186 (3), 1–9. https://link.springer.com/article/10.1007/s00604-019-3254-7.

Yuan, W., Ho, H.P., Lee, R.K., Kong, S.K., 2009. Surface-enhanced Raman scattering biosensor for DNA detection on nanoparticle island substrates. Appl. Optic. 48 (22), 4329–4337. https://www.osapublishing.org/ao/abstract.cfm?uri=ao-48-22-4329.

Zhang, Y., Huang, Y., Zhai, F., Du, R., Liu, Y., Lai, K., 2012a. Analyses of enrofloxacin, furazolidone and malachite green in fish products with surface-enhanced Raman spectroscopy. Food Chem. 135 (2), 845–850. https://www.sciencedirect.com/science/article/pii/S03088146 12007455.

Zhang, Y., Lai, K., Zhou, J., Wang, X., Rasco, B.A., Huang, Y., 2012b. A novel approach to determine leucomalachite green and malachite green in fish fillets with surface-enhanced Raman spectroscopy (SERS) and multivariate analyses. J. Raman Spectrosc. 43 (9), 1208–1213. https://onlinelibrary.wiley.com/doi/full/10.1002/jrs.4050.

Zhao, L., Jiang, D., Cai, Y., Ji, X., Xie, R., Yang, W., 2012. Tuning the size of gold nanoparticles in the citrate reduction by chloride ions. Nanoscale 4 (16), 5071–5076. https://pubs.rsc.org/en/content/articlehtml/2012/nr/c2nr30957b.